Calcif Tissue Int (1992) 51:78–82

Calcified Tissue International

Calcium Biomineralization in the Radular Teeth of the Chiton, *Acanthopleura hirtosa*

Louise A. Evans,[1] David J. Macey,[2] and John Webb[1]

Schools of [1]Mathematical and Physical Sciences and [2]Biological and Environmental Sciences, Murdoch University, Murdoch, Western Australia 6150, Australia

Received June 7, 1991, and in revised form September 4, 1991

Summary. A method has been devised for isolating the calcium biomineral from the iron biominerals and organic components present in the major lateral teeth of the chiton *Acanthopleura hirtosa*. Fourier-transform infrared spectroscopy of the calcium biomineral indicated that it was an apatite material containing carbonate and fluoride ions. Carbonate was not found to be present as a separate phase. The apatite was further separated into low and high density fractions, both of which showed crystallinity intermediate between that of bovine tibia cortical bone and human tooth enamel, as indicated by powder X-ray diffraction analysis. The calcified region of the major lateral teeth was also studied *in situ* using transmission electron microscopy and electron diffraction analysis, revealing a close spatial relationship between the mineral apatite phase and underlying organic matrix. It is suggested that the architectural arrangement of apatite biomineral and fibrous organic constituents imparts specialized mechanical properties to the tooth making it ideally suited for the task of obtaining food from hard surfaces.

Key words: Molluscs – Chiton radula – Apatite – Organic matrix.

The biomineralized teeth of chitons (Mollusca: Polyplacophora) are a unique example of invertebrate mineralized tissue in that in many species the teeth contain crystalline phases of both calcium phosphate and iron oxide biominerals. The teeth are borne on a radula or tongue which can be envisaged as a "conveyor belt" containing the teeth in various stages of development, ranging from soft organic structures at the posterior end of the radula through to fully mineralized teeth at the anterior end [1]. When fully formed, the mineralized major lateral teeth are used to scrape algae from the rocky substrate on which the animal lives [2].

Though the teeth are first mineralized with iron biominerals (ferrihydrite, $5Fe_2O_3.9H_2O$; magnetite, Fe_3O_4; goethite, α-FeO.OH; and lepidocrocite, γ-FeO.OH), these biominerals are restricted to the posterior region of the tooth [3]. In the latter stages of development, the remainder of the tooth becomes mineralized with an apatite material [4]. Once infilling of the anterior region has occurred, the calcium and iron biominerals are located in architecturally discrete compartments [4, 5].

A few studies have looked at the calcium biomineral contained in chiton teeth [4, 6], but these have been complicated by the presence of several iron phases together with large amounts of organic material. In addition, the presence of magnetite (Mohs hardness 6.0–6.5) has made thin sectioning of the teeth extremely difficult, thus preventing their examination at high magnification. Recent studies in our laboratories have concentrated on the chiton species *Acanthopleura hirtosa* (formerly *Clavarizona hirtosa* [7]). However, this work has focussed on the iron biominerals present [1], and relatively little is known concerning the accompanying calcium phase. In other chiton species, francolite, a carbonated fluorapatite [4], or dahllite, a carbonated hydroxyapatite [6], has been reported as the probable calcium biomineral. In the current study we present a method for removal of the iron biominerals present within the teeth of *A. hirtosa*, together with the subsequent identification and characterization of the calcium biomineral present using the combined techniques of electron microscopy, infrared spectroscopy, and electron and X-ray diffraction analyses.

Materials and Methods

Specimens of *A. hirtosa* were collected from intertidal rocks near the Perth metropolitan region (latitude 32° S, longitude 116° E) and their radulae were carefully removed. All radulae were cleaned briefly in 2% w/v NaOCl to remove overlaying cellular material. To preclude the presence of any precursors such as amorphous calcium phosphate [6] only the last 20 rows of teeth out of the total number of 70 were used in this study. Consequently, only mature teeth were examined in the current work.

Following dissection, radular segments were dialyzed against a solution of 35 mM sodium dithionite/6 mM 2,2′-dipyridyl in phosphate buffer (final pH 6.8) to remove iron. The system was stirred constantly and kept under nitrogen, with the demineralizing solution being changed daily. Removal of iron was confirmed by the formation of the intensely colored bisdipyridyliron(II) complex [8]. After 10 days of treatment, the freshly prepared iron-demineralizing solution remained colorless, indicating that all available iron had been removed. The segments were then dialyzed against two changes of buffer and several changes of distilled water before finally being removed from the dialysis bag and washed exhaustively with distilled water. Note that all solutions used, including washing solutions, were equilibrated with synthetic hydroxyapatite to minimize sample dissolution, as suggested by Weiner and Price [9].

For transmission electron microscopy (TEM), iron demineralized radular segments were dehydrated through a graded series of alcohols, transferred to propylene oxide, and infiltrated with an Epon-Araldite mixture by introducing the resin gradually over 5 days. Ultrathin sections were cut at 60–70 nm using a diamond knife (Dupont) on a Reichert-Jung OmU3 ultramicrotome. In order to provide a comparison, some sections were left unstained while others were treated with saturated aqueous uranyl acetate and lead

Offprint requests to: D. J. Macey

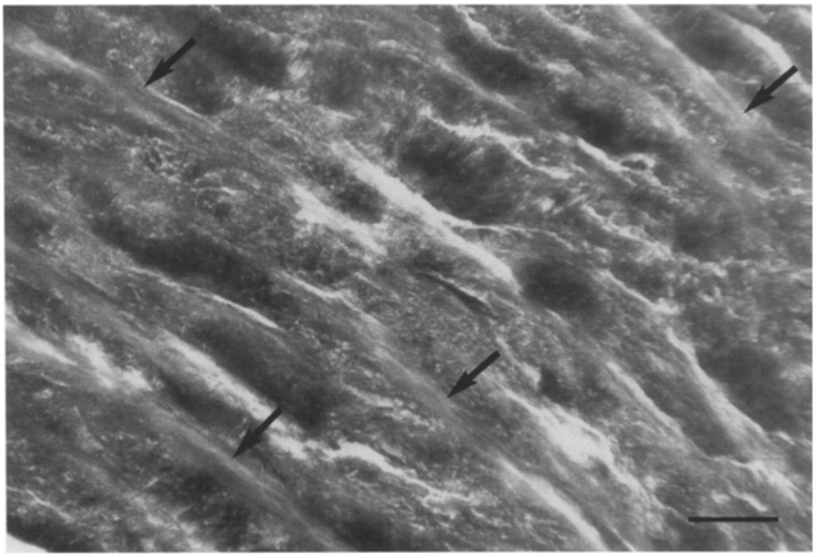

Fig. 1. Transmission electron micrograph of a stained longitudinal section of the calcified region of a major lateral tooth of *Acanthopleura hirtosa* showing the presence of mineralized areas between parallel organic fibers (arrows). Note that the long axis of the fibers was seen to be oriented approximately perpendicular to the anterior surface. Scale bar 2 μm.

citrate [10]. TEMs and electron diffraction patterns were obtained using a Philips 301 electron microscope operating at 80 keV. Electron micrographs were taken of both unstained and stained sections whereas only unstained sections were used for electron diffraction analyses. Interplanar spacings were calculated using the camera length determined from diffraction patterns of standard material (evaporated TlCl; TAAB, Reading). The lattice spacings thus obtained were compared with Joint Committee on Powder Diffraction Standards (JCPDS) data for apatite minerals and with patterns obtained from synthetic hydroxyapatite (see below).

For analysis of the calcium biomineral by Fourier-transform infrared spectroscopy (FT-IR) and powder X-ray diffraction (XRD), iron demineralized radular segments were treated according to Method 1 of Weiner and Price [9] which uses a 2.6% w/v NaOCl solution to remove organic constituents. In addition, to further separate the inorganic components obtained using this method, the material was placed into a conical tube with water and vortexed. After allowing the sample to settle for 60 seconds, the supernatant was transferred to a second tube and centrifuged at 2,000 *g* for 3 minutes. The vortexing and centrifuging steps were repeated several times. Using these techniques, comparable amounts of a white material and an off-white heavier material were obtained. The material from both fractions was then washed with distilled water and ethanol, dried, and analyzed.

FT-IR analyses were undertaken on 13-mm pellets (2 mg sample/300 mg KBr) using a Perkin Elmer 1720-X spectrometer. XRD analyses were obtained with a Philips PW1700 automated powder diffractometer using Ni-filtered Cu K_α radiation generated at 45 kV, 40 mA with a scanning speed of 0.125°/minute. Interplanar spacings were determined from 2Θ values obtained using Si as a standard. Miller indices were assigned by comparison of interplanar spacings with those from appropriate JCPDS cards [11]. Lattice parameters were calculated from the (410) and (300) reflections (a-axis) and from the (004) and (002) reflections (c-axis) using a hexagonal indexing system [12].

Reference material for FT-IR and XRD analyses was prepared from caries-free adult human teeth using a tetrabromoethane flotation method (d 2.7 g-cm^{-3}) [13] to separate enamel from dentine. Bovine tibia cortical bone was prepared using NaOCl solution to remove organic components [9]. Synthetic stoichiometric hydroxyapatite was a high-temperature (1100–1200°C), nonaqueous preparation [13]. In order to check that the apatite was not affected by the iron demineralization procedure or by the water treatment, samples of human enamel and dentine and bovine tibia cortical bone were treated with dithionite/dipyridyl and then washed by vortexing and centrifuging with hydroxyapatite equilibrated water as given above. The FT-IR spectra of the treated material was then compared with those obtained from untreated material. In each case, spectra obtained from treated material were identical in every respect with those obtained from untreated material, including sharpness of spectral patterns, band position, and band intensity. In addition, treated reference material did not separate into different fractions as occurred in the case of chiton radular material, indicating that fractionation of the chiton material was not due to either the iron demineralization or the water treatments.

Results

TEM showed that the calcified region of the major lateral teeth of *A. hirtosa* consisted mostly of strands of organic material arranged in a parallel fashion and separated by heavily mineralized elongated areas (Fig. 1). Areas deep within the tooth cusp appeared to be less extensively mineralized, and at high magnification it was apparent that in these areas the mineral deposits were composed of aggregates of crystals ranging in size from 10 to 20 nm (Fig. 2). In some cases the crystals could be seen to be arranged in a regular pattern surrounding a central unmineralized zone. This central unmineralized zone was thought to correspond in both position and size to the finer organic fibers which have been described previously in the organic matrix of *A. hirtosa* [14]. In unstained sections, these less densely mineralized areas afforded selected-area electron diffraction analysis. The electron diffraction pattern obtained was consistent with that of an apatite material (Fig. 2). In addition, marked variation in the intensity of the inner 002 reflection was noted (Fig. 2).

FT-IR spectra of both low and high density chiton mineral fractions obtained following chemical isolation of the calcium biomineral showed marked similarities to spectra derived from the series of biogenic carbonate-substituted hydroxyapatites used as reference material (Fig. 3). However, absorption bands due to CO_3^{2-} (1450, 1410, and 870 cm^{-1}) were more intense in the spectra of bovine tibia cortical bone and human tooth enamel compared with those of chiton. In addition, chiton spectra showed a distinct shoulder at about 575 cm^{-1}. All of the biological apatites showed an increase in C-O absorption intensity in the 1500–1400 cm^{-1} region, together with a marked decrease at 634 cm^{-1} when compared with spectra obtained from synthetic stoichiometric

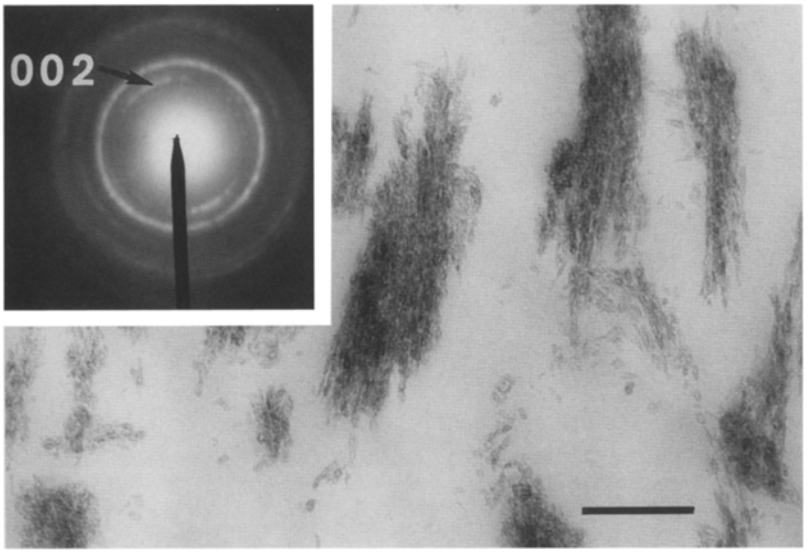

Fig. 2. Transmission electron micrograph of the calcified region deeper in the cusp showing crystal aggregates. In many areas groups of crystals can be seen arranged in a circular pattern around an inner unmineralized region. Scale bar 200 nm. Inset: Electron diffraction pattern obtained from a sparsely mineralized area. Note the oriented arc of the 002 reflection.

apatite. None of the apatite samples showed any absorption in the 720–700 cm^{-1} (CO_3^{2-} ν_4) region.

XRD analysis of both chiton calcium mineral fractions showed patterns characteristic of an apatite material. In addition, the analysis indicated that the fractions differed in their crystallinity. The crystallinity of both low and high density chiton fractions, as indicated by peak broadening, was intermediate between that of human tooth enamel and bovine tibia cortical bone (Fig. 4). The lattice constants of *A. hirtosa* apatite were calculated to be a = 9.387 (±0.005) Å and c = 6.866 (±0.005) Å.

Discussion

This study has indicated that, in addition to iron, the major lateral teeth of the chiton *A. hirtosa* are mineralized with an apatite material containing both carbonate and fluoride ions as discussed below. The presence of carbonate in chiton apatite has previously only been inferred when it was noted that the teeth of *A. echinatum* liberated carbon dioxide when treated with hydrochloric acid [4].

The greater intensity of absorption bands due to CO_3^{2-} in FT-IR spectra of bone and enamel reflect a higher carbonate content in these samples relative to that of chiton. Values of approximately 2.5% w/w carbonate have been reported for enamel [15] although this value may vary between individuals. The absence of a CO_3^{2-} ν_4 band in the IR spectra of biological apatites has been shown to indicate that carbonate is present as an intrinsic part of the apatite structure and not as a separate calcium carbonate phase [16]. In addition, the increased absorption at 634 cm^{-1} for synthetic hydroxyapatite when compared with biological apatites has been attributed to hydroxyl ion deficiencies in the structure of carbonated apatites [13].

A distinct shoulder at 575 cm^{-1} in the IR spectra of apatites has been attributed to Cl^- or F^- substitution for OH^- [17]. Since influx of fluorine, as opposed to chlorine, has been identified by elemental analysis of mature radular segments of *A. hirtosa* using PIGME (proton-induced γ-ray emission) [18], this shoulder is most probably due to fluoride substitution in the apatite of *A. hirtosa*. The PIGME work, however, included organic material and iron minerals in the analyses and thus could not provide conclusive evidence that the fluoride was actually incorporated into the calcium biomineral. In this context it should be noted that a shoulder at 575 cm^{-1} attributed to fluoride incorporation has also been found in the IR analysis of brachiopod shell apatite [19]. In an *in situ* study of the calcium biomineral in the teeth of the chiton *A. haddoni,* Lowenstam and Weiner [6] were only able to examine IR absorption bands in the 800–475 cm^{-1} region, as this is the only area free of additional absorption due to the organic components. In this study, a shoulder at 575 was also observed, but these authors identified the calcium biomineral present as dahllite, a carbonated hydroxyapatite mineral, rather than as francolite, a carbonated fluorapatite. It is also interesting to note that the relative intensity of the C-O bands at 1450 and 1410 cm^{-1} for *A. hirtosa* apatite is similar to that obtained for synthetically derived carbonate- and fluoride-containing apatites, whereas those in bovine tibia and human tooth enamel more closely resemble that obtained for synthetic apatite containing only carbonate (LeGeros, personal communication). These observations further suggest that *A. hirtosa* apatite contains both carbonate and fluoride ions.

The smaller unit cell dimensions calculated for chiton apatite (a = 9.387, c = 6.866 Å) compared with human enamel (a = 9.441, c = 6.882 Å) can be explained by appreciable fluoride-substitution in the apatite of *A. hirtosa*. Previous studies have noted that carbonate substitution results in a shortening of the a-axis and expansion in the c-axis whereas fluoride substitution causes a contraction in the a-axis but does not affect the c-axis [16, 19]. In this regard, *A. hirtosa* apatite is similar to the mineral francolite, a carbonate-containing fluorapatite. We note that the lattice parameters for *A. hirtosa* apatite are similar to those reported for shell apatite in the inarticulate brachiopod, *Lingula unguis* [20].

The difference in crystallinity between the two apatite fractions in *A. hirtosa* may be due to variations in the degree of fluoride and carbonate substitution and/or to the occurrence of different crystal sizes within the teeth. Significant differences either in the chemical nature or in the degree of substitution of the two apatites would be reflected by a shift in position of at least some of the X-ray diffraction peaks. Because the 2Θ values obtained from XRD analysis of both

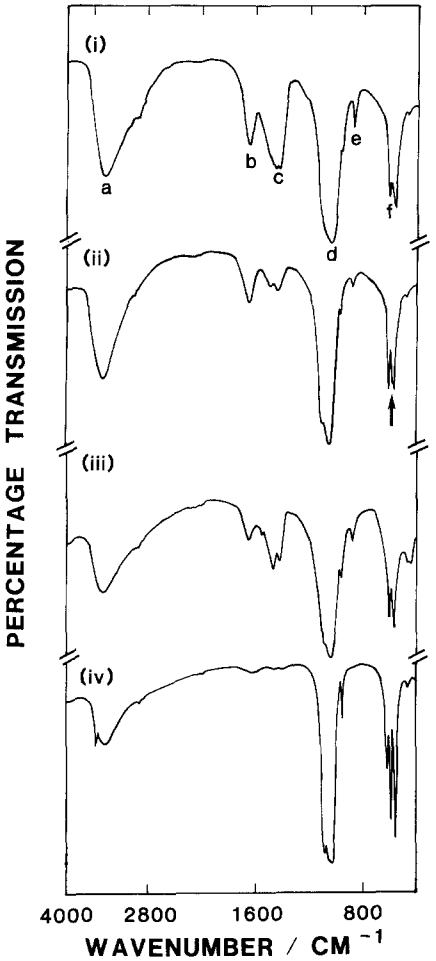

Fig. 3. Fourier-transform infrared spectra obtained from NaOCl extracted material from (i) bovine tibia cortical bone, (ii) chiton major lateral teeth, (iii) human tooth enamel, and (iv) stoichiometric synthetic apatite. Absorption bands are due to the following groups: (a) H_2O, (b) H_2O, (c) CO_3, (d) PO_4, (e) CO_3, (f) PO_4. The distinct shoulder exhibited by chiton apatite at 575 cm^{-1} is arrowed in (ii). Note that the sharp band at 3572 cm^{-1} in (iv) is due to an OH stretching vibration.

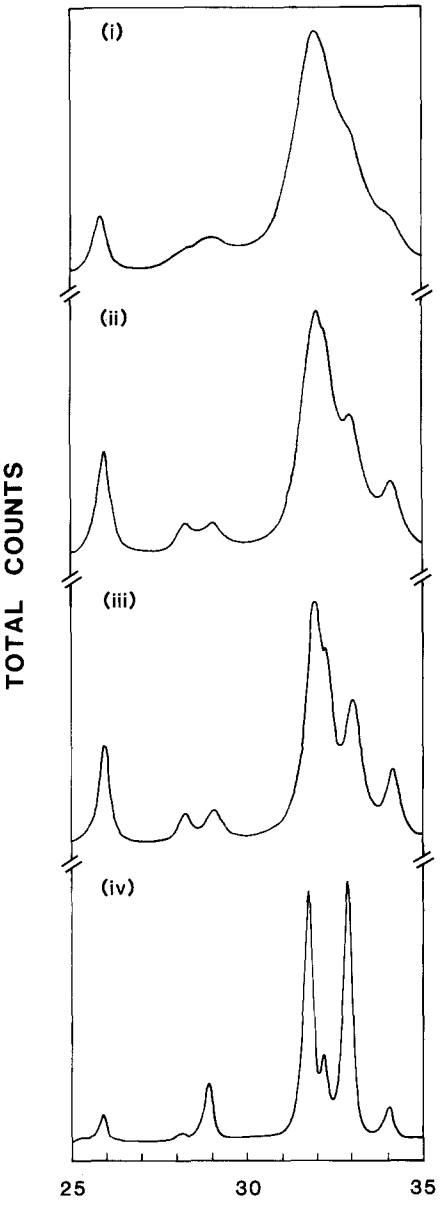

Fig. 4. X-ray powder diffraction patterns of (i) bovine tibia cortical bone, (ii) chiton major lateral teeth (low density fraction), (iii) chiton major lateral teeth (high density fraction), and (iv) human tooth enamel. Note the increase in crystallinity from (i) to (iv) as denoted by the decrease in broadening of the diffraction peaks. In addition, the differences observed in relative peak intensities in pattern (iv) is due to preferred crystal orientation in the case of the enamel specimen.

low and high density fractions were extremely similar, it is likely that the differences observed in the sharpness of diffraction patterns were due to crystal size. Although only small (10–20 nm) individual crystals were seen deep within the cusp in the present study, a previous study of partially demineralized teeth identified larger acicular crystals approximately 150–200 nm in length which occurred towards the surface of the anterior region [14]. It is thus possible that crystal size is related to position within the tooth structure. In this context, three types of apatite crystals differing in size and shape have been noted in the shell of *L. unguis* [21]. However, these authors noted that crystal size increased towards the central part of the shell.

The variation in intensity of the 002 reflection in electron diffraction patterns obtained from material *in situ* indicated preferred orientation of the c-axis of *A. hirtosa* apatite crystals. This is in contrast to the iron mineralized region of the tooth in which magnetite deposits are randomly organized [1]. Similar results have been obtained using X-ray diffraction analysis for dahllite crystals in the teeth of *A. haddoni* [6]. These authors also noted the lack of preferred orientation of the magnetite deposits in their species.

The overall pattern of calcification seen at the TEM level reflects the results obtained in an earlier study into the organic matrix of the teeth of *A. hirtosa* [14]. This previous study showed the presence of highly organized organic fibers in the anterior region of the tooth, which appeared as thick parallel fibers interconnected by a meshwork of finer fibers. The present study has confirmed that mineral deposition occurs between the thicker parallel fibers. In addition, the ar-

rangement of individual apatite crystals around a central unmineralized core seen in unstained sections is almost certainly due to the formation of crystals around the finer matrix fibers. Thus, crystal deposition is closely associated with the fine fibrous constituents of the organic matrix. The occurrence of large amounts of organic material in the calcified region of the tooth is in contrast to the magnetite-bearing region in which fibers are sparsely distributed [14, 22]. The higher organic content in the calcified region is thought to impart tensile strength to the tooth, allowing plastic deformation to occur before material failure [14, 23]. In the teeth of this chiton species, the combination of an organic-rich calcified anterior region that supports the harder iron-rich posterior region results in the formation of an effective structure for the excavation of hard substrates.

Acknowledgments. We thank G. Thomson, D. A. Clarke, P. Fallon, and Drs. T. G. St. Pierre, N. D. Chasteen, and R. Chang for their excellent technical assistance, together with Professor R. Z. LeGeros for helpful comments on the manuscript. We also thank B. Cockman for the sample of human teeth and Drs. B. E. Williamson and D. G. A. Nelson for the sample of stoichiometric apatite. The award of an Australian Postgraduate Research Award to LA Evans together with funding from Murdoch University's Special Research Grant and the Australian Research Council are gratefully acknowledged.

References

1. Kim K-S, Macey DJ, Webb J, Mann S (1989) Iron mineralization in the radula teeth of the chiton *Acanthopleura hirtosa*. Proc R Soc Lond B 237:335–346
2. Steneck RS, Watling L (1982) Feeding capabilities and limitation of herbivorous molluscs: a functional group approach. Mar Biol 68:299–319
3. Webb J, Macey DJ, Mann S (1989) Biomineralization of iron in molluscan teeth. In: Mann S, Webb J, Williams RJP (eds) Biomineralization: chemical and biochemical perspectives. VCH Verlagsgesesellschaft, Weinheim, pp 345–387
4. Lowenstam HA (1967) Lepidocrocite, an apatite mineral, and magnetite in teeth of chitons (Polyplacophora). Science 156:1373–1375
5. Evans LA, Macey DJ, Webb J (1991) Distribution and composition of matrix protein in the radula teeth of the chiton *Acanthopleura hirtosa*. Mar Biol 109:281–286
6. Lowenstam HA, Weiner S (1985) Transformation of amorphous calcium phosphate to crystalline dahllite in the radular teeth of chitons. Science 227:51–53
7. Ferreira AJ (1986) A revision of the genus *Acanthopleura* Guilding, 1829 (Mollusca: Polyplacophora). The Veliger 28:221–279
8. Svehla G (1979) Vogel's textbook of macro and semimicro qualitative inorganic analysis, 5th ed. Longman, London, p 244
9. Weiner S, Price PA (1986) Disaggregation of bone into crystals. Calcif Tissue Int 39:365–375
10. Reynolds ES (1963) The use of lead citrate and high pH as an electron-opaque stain in electron microscopy. J Cell Biol 17:208–212
11. Joint Committee on Powder Diffraction Standards (1980) Mineral powder diffraction file data book. International center for diffraction data, Swarthmore, USA
12. Azároff LV, Buerger MJ (1958) The powder method in X-ray crystallography. McGraw-Hill, New York
13. Nelson DGA, Williamson BE (1982) Low-temperature laser Raman spectroscopy of synthetic carbonated apatites and dental enamel. Aust J Chem 35:715–727
14. Evans LA, Macey DJ, Webb J (1990) Characterization and structural organization of the organic matrix of the radula teeth of the chiton *Acanthopleura hirtosa*. Phil Trans R Soc Lond B 329:87–96
15. Zapanta-LeGeros R (1965) Effect of carbonate on the lattice parameters of apatite. Nature 206:403–404
16. LeGeros RZ, LeGeros JP, Trautz OR, Klein E (1970) Spectral properties of carbonate in carbonate-containing apatites. Dev Appl Spec 7:3–12
17. LeGeros RZ (1974) The unit-cell dimensions of human enamel apatite: effect of chloride incorporation. Archs Oral Biol 20:63–71
18. Kim K-S, Webb J, Macey DJ, Cohen DD (1986) Compositional changes during biomineralization of the radula of the chiton *Clavarizona hirtosa*. J Inorg Biochem 28:337–345
19. LeGeros RZ, Pan C-M, Suga S, Watabe N (1985) Crystallochemical properties of apatite in atremate brachiopod shells. Calcif Tissue Int 37:98–100
20. Iijima M, Moriwaki Y (1990) Orientation of apatite and organic matrix in *Lingula unguis* shell. Calcif Tissue Int 47:237–242
21. Iijima M, Moriwaki Y, Gyōtoku T, Hayashi K, Imaru S (1989) Small angle X-ray scattering study on *Lingula unguis* shell. Jpn J Oral Biol 31:308–316
22. Webb J, Evans LA, Kim K-S, St Pierre TG, Macey DJ (1991) Controlled deposition and transformation of iron biominerals in chiton radula teeth. In: Suga S, Nakahara H (eds) Mechanisms and phylogeny of mineralization in biological systems. Springer-Verlag, Tokyo, pp 283–290
23. Birchall JD (1989) The importance of the study of biominerals to materials technology. In: Mann S, Webb J, Williams RJP (eds) Biomineralization: chemical and biochemical perspectives. VCH Verlagsgesellschaft, Weinheim, pp 491–509